

Characterizing Concentrated, Multiply Scattering, and Actively Driven Fluorescent Systems with Confocal Differential Dynamic Microscopy

Peter J. Lu (陸述義),¹ Fabio Giavazzi,² Thomas E. Angelini,¹ Emanuela Zaccarelli,³ Frank Jargstorff,⁴ Andrew B. Schofield,⁵ James N. Wilking,¹ Mark B. Romanowsky,¹ David A. Weitz,¹ and Roberto Cerbino²

¹*Department of Physics and SEAS, Harvard University, Cambridge, Massachusetts 02138, USA*

²*Dipartimento di Chimica, Biochimica e Biotecnologie per la Medicina, Università degli Studi di Milano, I-20090, Italy*

³*CNR-ISC and Dipartimento di Fisica, Università di Roma La Sapienza, I-00185 Rome, Italy*

⁴*NVIDIA, Santa Clara, California 95050, USA*

⁵*Department of Physics, University of Edinburgh, Edinburgh EH9 3JZ, United Kingdom*

(Received 3 June 2010; revised manuscript received 21 February 2012; published 22 May 2012)

We introduce confocal differential dynamic microscopy (ConDDM), a new technique yielding information comparable to that given by light scattering but in dense, opaque, fluorescent samples of micron-sized objects that cannot be probed easily with other existing techniques. We measure the correct wave vector q -dependent structure and hydrodynamic factors of concentrated hard-sphere-like colloids. We characterize concentrated swimming bacteria, observing ballistic motion in the bulk and a new compressed-exponential scaling of dynamics, and determine the velocity distribution; by contrast, near the coverslip, dynamics scale differently, suggesting that bacterial motion near surfaces fundamentally differs from that of freely swimming organisms.

DOI: [10.1103/PhysRevLett.108.218103](https://doi.org/10.1103/PhysRevLett.108.218103)

PACS numbers: 87.64.mk, 47.57.E-, 78.35.+c, 82.70.Dd

Fluorescence imaging is an important and versatile form of optical microscopy. Fluorescent tags can selectively identify specific features within an image, thereby enhancing contrast; this is particularly powerful in biology and soft-matter physics. A major difficulty, however, is that all fluorescent objects within the illumination beam emit light, even if outside the microscope's focal plane, hindering collection of high-quality images. Using a confocal pinhole, which limits detected light to only that originating from the focal plane, confocal microscopy allows true 3D imaging. By its very nature, however, confocal microscopy is relatively slow; collecting a 3D stack of images usually requires several seconds, limiting the study of dynamics to relatively slow phenomena, characterized by time scales well in excess of a second [1,2].

Even traditional bright field microscopy is limited in its ability to follow rapid dynamics; by contrast, another optical method, dynamic light scattering (DLS), is well-suited to characterize dynamics at high speeds, specifically ensemble averages as a function of scattering wave vector q , albeit at the cost of losing real-space information [3]. One way to combine DLS with the advantages of real-space imaging in the wide field is differential dynamic microscopy (DDM), which extends to lower- q information analogous to that given by DLS [4–6]. However, DDM has thus far been restricted to wide field imaging; consequently, like DLS, DDM probes only dilute suspensions [4–6]. No equivalent method exists for fluorescence, particularly in high-concentration samples where imaging is obscured. This severely limits the use of fluorescence microscopy for studies of dynamics in dense samples.

In this Letter, we introduce a new technique using confocal fluorescence microscopy that provides a powerful probe not only of rapid dynamics but also of the static structure of dense, fluorescent samples that multiply scatter light, precluding their study with other techniques. Motivated by DDM analysis, we examine the Fourier spectra of the differences between pairs of images within a sequence; the short-time differences confirm diffusive motion of hard-sphere-like colloidal suspensions, even at volume fractions ϕ far higher than those that can be measured accurately with DLS and DDM; our measured diffusion coefficient is in good agreement with the value determined by using other techniques. Moreover, confocal microscopy allows a sufficient signal, even in these dense samples, to measure meaningfully the difference between image pairs separated by long-time delays. This provides information on static structure, analogous to that given by static light scattering (SLS), but here for highly concentrated samples that multiply-scatter light; our measurement of the static structure factor $S(q)$ in colloidal suspensions is in quantitative agreement with theory and independent measurements. Furthermore, we combine these measurements to probe particle interactions: Our purely experimental determinations of the hydrodynamic factor $H(q)$ are in quantitative agreement with theory, which has not been achieved with any light-based technique for such dense suspensions. To illustrate further the technique's power, we apply it to an actively driven, biological system: dense, macroscopically opaque suspensions of fluorescent bacteria swimming freely. We observe new scaling of dynamics that depends on the distance from the coverslip, a new phenomena in the bulk not seen when organisms swim in a 2D plane near the coverslip,

and determine the distribution of swimming velocities. We term this technique, which enables these measurements, confocal differential dynamic microscopy (ConDDM).

Our confocal fluorescence microscope includes a Nipkow spinning disk [Yokogawa], CCD camera [QImaging], 100 \times oil 1.4 N.A. objective [Leica], solid-state 532-nm laser [Laserglow], and hardware timing control [1]. We suspend spheres of sterically stabilized polymethylmethacrylate (PMMA) with DiIC18 dye [2] in a solvent of 18% (by mass) cis-decahydronaphthalene, 22% tetrahydronaphthalene, and 60% tetrachloroethylene. At 25 $^{\circ}$ C, the solvent has density 1.280 ± 0.002 g/cm 3 , dynamic viscosity 1.288 ± 0.002 mPa sec, and refractive index $n = 1.505$; particles remain neutrally buoyant for days and are macroscopically transparent at close-packed densities.

We collect multiple uninterrupted sequences of >1000 images of 256×256 pixels, from a depth 20 μ m from the coverslip, at 33.4 frames per sec; a typical image from the sample at $\phi = 0.20$ is shown in Fig. 1(a). We select pairs of images separated by a time interval δt and subtract one from the other, removing any time-independent background, shown for $\delta t = 0.06$, 0.25, and 1.00 sec in Figs. 1(b)–1(d), respectively. We calculate the 2D Fourier

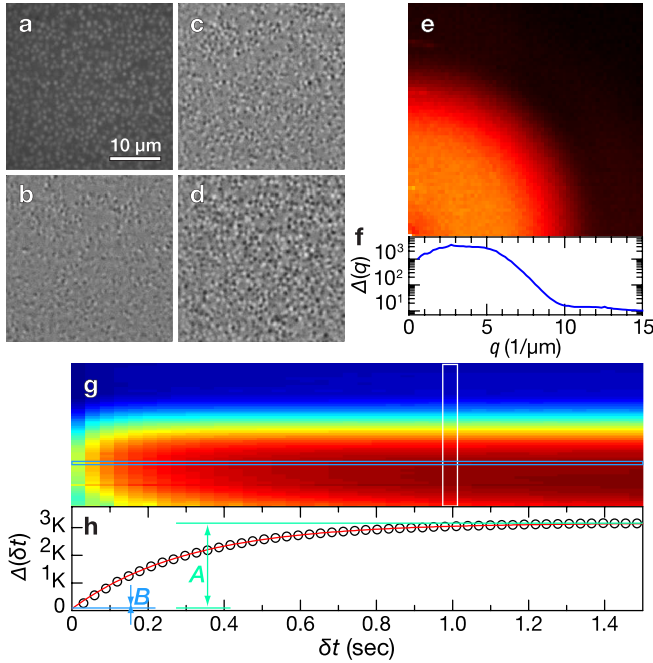


FIG. 1 (color online). (a) Raw confocal fluorescence image of particles at $\phi = 0.20$. Difference between images separated in time by (b) $\delta t = 0.06$ sec, (c) $\delta t = 0.25$ sec, and (d) $\delta t = 1.00$ sec. (e) 2D $\bar{\Delta}(\vec{q}, \delta t = 1.00$ sec) averaged over 10^4 image pairs and (f) its 1D azimuthal average $\Delta(q, \delta t = 1.00$ sec) plotted on the same scale in q . (g) $\Delta(q, \delta t)$, where the function in (f) corresponds to the white rectangle. (h) $\Delta(q = 3.9 \mu\text{m}^{-1}, \delta t)$ shows the time evolution at constant $q = 3.9 \mu\text{m}^{-1}$ and corresponds to the blue rectangle in (g).

transform of this difference, square its magnitude to give a 2D power spectrum as a function of wave vector $\vec{q} = (q_x, q_y)$, and average for all image pairs of equal δt within the sequence [4,5] to yield $\bar{\Delta}(\vec{q})$, shown for 10^4 image pairs in Fig. 1(e) for $\delta t = 1.00$ sec. The original implementation of this algorithm [MATLAB] requires several hours of computation for typical image sequences; however, the numerous independent fast Fourier transforms (FFT) and image pair subtractions make this calculation well-suited to parallelization. Therefore, we implement the same algorithm on a graphics processing unit (GPU) [NVIDIA Tesla C2050 GPU, CUDA C, CuFFT, NPP]; our accelerated code is 2 orders of magnitude faster, reducing processing time to around a minute, making the experiment far more interactive.

The sample dynamics and structure are isotropic, evidenced by the circular symmetry of $\bar{\Delta}(\vec{q})$ in Fig. 1(e); therefore, we average azimuthally to determine $\Delta(q)$ as a function of scalar wave vector magnitude $q \equiv (q_x^2 + q_y^2)^{1/2}$, shown in Fig. 1(f). Repeating this procedure for different δt yields the image structure function $\Delta(q, \delta t)$, shown in Fig. 1(g), where the slice outlined by the vertical (white) rectangle corresponds to $\Delta(q, \delta t = 1.00$ sec) in Fig. 1(f). To probe temporal dependence, for each q we slice $\Delta(q, \delta t)$ along the δt axis; the data from one slice, outlined by the horizontal (blue) rectangle in Fig. 1(g), represent sample time evolution at fixed $q = 3.9 \mu\text{m}^{-1}$ and are marked with symbols in Fig. 1(h). For $\delta t = 0$, $\Delta(q, \delta t \rightarrow 0) = B(q)$, a time-independent noise floor; as δt increases, the differences between images in each pair increase. Consequently, $\Delta(q, \delta t)$ rises until saturating when the images are totally decorrelated, following the form $\Delta(q, \delta t) = 2A(q)[1 - g(q, \delta t)] + B(q)$, where the image correlation function $g(q, \delta t)$ is equivalent to the intermediate scattering function in DLS. For dilute Brownian particles, $g(q, \delta t) \equiv \exp[-\delta t/\tau(q)]$, where $\tau_{\text{dil}}(q) \equiv 1/(D_0 q^2)$ and D_0 is the single-particle diffusion coefficient [4,5]; our experimental data conform closely to this exponential form, shown with the solid curve in Fig. 1(h). We repeat the fit for each q to yield estimates of $A(q)$, $B(q)$, and $\tau(q)$. The fit is valid when $q > q_{\text{min}} \equiv 2\pi/L = 0.2 \mu\text{m}^{-1}$, where L is the image size, and when $q < q_{\text{max}} = 8 \mu\text{m}^{-1}$. In general, q_{max} is set by the minimum distance particles move between successive frames, though here q_{max} coincides with a particle form-factor minimum, shown with a dotted gray line in Fig. 3(a); these q values map to scattering angles between 0.4° and 25° , well below those accessed easily with traditional light scattering setups.

At high $q \rightarrow q_{\text{max}}$, the $\tau_{\text{dil}}(q)$ data from a dilute sample at $\phi = 0.005$ scale as q^{-2} , as in DDM, shown with downward-pointing (blue) triangles in Fig. 2; the fit to the data yields $D_0 = 0.338 \pm 0.005 \mu\text{m}^2/\text{s}$. For comparison, we measure a dilute sample at $\phi < 0.001$ of the same particles and solvent with DLS [ALV], which fall

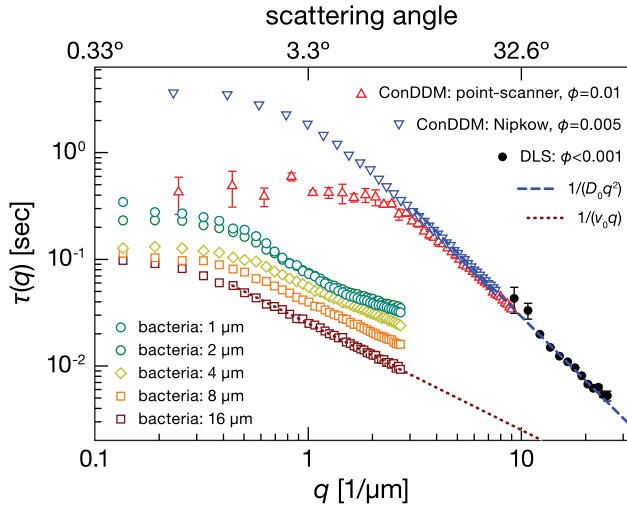


FIG. 2 (color online). $\tau(q)$ for dilute colloidal suspensions, using data from a Nipkow-disk confocal (open blue downward-pointing triangles), point-scanning confocal (open red upward-pointing triangles), and DLS (filled black circles), scale at high q as q^{-2} and fall on the same (dashed blue) line. At low q , the Nipkow-disk data plateau to a far higher value than that from the point scanner, demonstrating the latter's higher resolution along the optical axis. For swimming bacteria, $\tau(q)$ data collected deep in the bulk, more than $4 \mu\text{m}$ from the coverslip (open diamonds and squares) scale at high q as q^{-1} (dotted line), indicating ballistic motion; by contrast, data from bacteria within $1\text{--}2 \mu\text{m}$ of the coverslip (open circles) follow no clear power law but instead are sigmoidal curves with inflection points near $q \approx 0.8 \mu\text{m}^{-1}$.

on the same dashed line shown in Fig. 2; the fit yields $D_0^{\text{DLS}} = 0.330 \pm 0.01 \mu\text{m}^2/\text{s}$, in quantitative agreement with the ConDDM-derived value, and a particle hydrodynamic radius $a_h = 508 \pm 6 \text{ nm}$ via the Stokes-Einstein relation. By contrast, at low q , confocal sectioning causes $\tau(q)$ in ConDDM to plateau to a constant $\tau(q \rightarrow 0) \equiv \tau_z \approx 6 \text{ sec}$, roughly the time for particles to diffuse out of the confocal imaging plane, similar to fluorescence correlation spectroscopy [3]. We estimate $\tau_z \approx (\delta z)^2/D_0$, where $\delta z \approx 1.5 \mu\text{m}$ approximates the confocal slice thickness; separately, we measure the full width at half maximum (FWHM) of the axial point-spread function, by dispersing quantum dots on a coverslip, and find it to be $1.6 \pm 0.1 \mu\text{m}$, comparable to δz . To test whether the plateau reflects generally the confocal \hat{z} resolution, we repeat the measurements with a different confocal microscope: a resonant-galvanometer point scanner with $63\times$ oil 1.4 N.A. objective [Leica], collecting at 55.0 fps with a 0.5 Airy-disk pinhole. At high q , the $\tau(q)$ data completely overlap the Nipkow and DLS data, shown with upward-pointing (red) triangles in Fig. 2; by contrast, at low q , we find $\delta z \approx 0.5 \mu\text{m}$, close to the measured FWHM of $0.52 \pm 0.01 \mu\text{m}$. These data demonstrate the novel ability of ConDDM to characterize the effective *in situ* point-spread function using any confocal microscope.

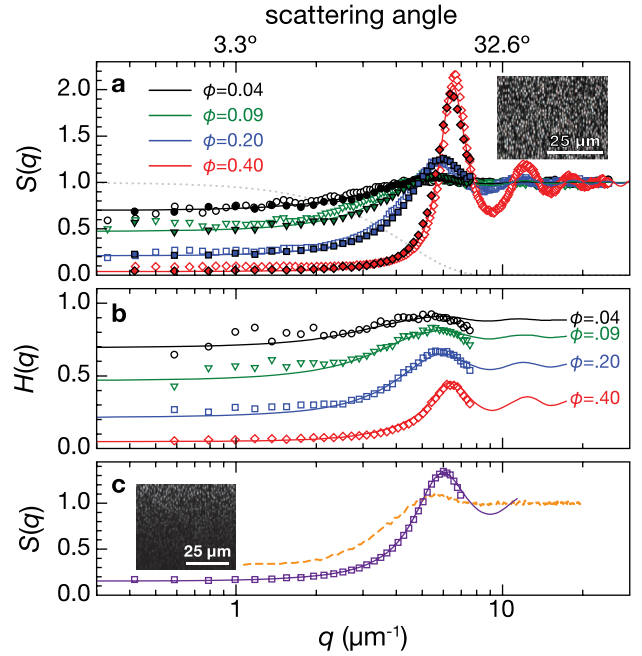


FIG. 3 (color online). (a) $S(q)$ for index-matched colloidal suspensions, from ConDDM (closed symbols), 3D particle positions (open symbols), and the PY model (solid curves). Particle form factor shown as a gray dotted line. (Inset) \hat{x} - \hat{z} image of the indexed-matched sample at $\phi = 0.40$ shows constant contrast $50 \mu\text{m}$ into the sample. (b) $H(q)$ for the same suspensions, from ConDDM (open symbols) and a theoretical model (solid curves). (c) $S(q)$ for an opaque, index-mismatched colloidal suspension at $\phi = 0.25$ (open squares). The PY prediction (solid curve) is in quantitative agreement with the data, while $S(q)$ from 3D particle positions (dashed curve) is completely different. (Inset) \hat{x} - \hat{z} image of the indexed-mismatched sample at $\phi = 0.25$ shows complete loss of contrast tens of microns into the sample.

Confocal sectioning allows enough signal to measure meaningfully the long-time limit $A(q)$ in dense samples, a new capability not possible in wide field DDM. In general, $A(q) \equiv \phi P(q)S(q)T(q)$, where $P(q)$ is the single-particle form factor, $S(q)$ the structure factor, and $T(q)$ the imaging-system transfer function [5]. $P(q)$ and $T(q)$ are fixed for samples with the same particles and solvents. For dilute $\phi \rightarrow 0$ suspensions, $S_{\text{dil}}(q) = 1$ and $A_{\text{dil}}(q) = \phi_{\text{dil}}T(q)P(q)$; therefore, we can determine $S(q)$ at any ϕ : $S(q) = \phi_{\text{dil}}A(q)/\phi A_{\text{dil}}(q)$, as shown with filled symbols in Fig. 3(a). We compare these measured data to theoretical $S(q)$ estimates within the Percus-Yevick (PY) model; the PY calculations are in excellent quantitative agreement with our data, shown with solid curves in Fig. 3(a); in all cases, the fits yield an estimate of particle radius $a_{\text{PY}} = 510 \pm 5 \text{ nm}$, within an error of a_h . To compare with traditional confocal microscope usage, we collect 3D stacks of these indexed-matched colloids, determine 3D particle positions with software [1], and calculate $S(q)$ with a discrete sum [2]. In all cases, the 3D data are slightly noisier but still in good agreement with both

the ConDDM data and PY calculation, as shown with open symbols in Fig. 3(a).

Simultaneously determining the DLS-like dynamic $\tau(q)$ (Fig. 2) and SLS-like static $S(q)$ [Fig. 3(a)] provides a tantalizing new way to measure hydrodynamics directly, with no additional data. For diffusing spheres, $g(q, \delta t)$ is an exponential at any ϕ for δt less than the Brownian time $\tau_B \equiv 4a^2/D_0$ [7]; $g_s(q, \delta t) \cong \exp[-\delta t/\tau_s(q)]$, where $\tau_s(q) = (D_0 q^2)^{-1} S(q)/H(q)$, and the hydrodynamic factor $H(q)$ characterizes hydrodynamic interactions among particles [7,8]. We find that $H(q)$ remains below 1 and decreases with increasing ϕ , expected for hard spheres [7] and consistent with previous x-ray photon correlation spectroscopy measurements [8], as shown with open symbols in Fig. 3(b). We compare our $H(q)$ data with theoretical predictions for hard spheres [9], marked with curves in Fig. 3(b), which are all in excellent agreement with our experimental data. Previous $H(q)$ estimates derived from light scattering assume a theoretical $P(q)$ [7]; by contrast, our purely experimental technique makes no such assumptions. Moreover, the quantitative agreement between experimental and theoretical $S(q)$ and $H(q)$ persists through the entire q range and will do so as long as $a_h \leq \delta z$ (Supplemental Material [10]); this agreement is especially striking at low q , inaccessible to light scattering, and high ϕ , not probed easily with fluorescence correlation spectroscopy.

The confocal pinhole's rejection of out-of-plane light permits observation deep in the bulk of fluorescent samples, even when they scatter light; therefore, ConDDM might provide new capabilities to make these light-scattering-like measurements in dense samples that scatter light multiply, not possible with DDM or traditional light scattering. To test this, we create a colloidal suspension with different solvents (1:3 dodecane:tetrachloroethylene) that closely matches the particles' density, but with $n = 1.47$ so strongly mismatches their refractive index that suspensions at $\phi = 0.25$ are macroscopically opaque. Here, particles near the coverslip can be resolved individually; those greater than $30 \mu\text{m}$ away are indistinguishable from the noise, as shown in the inset in Fig. 3(c). Using ConDDM, we measure $S(q)$ and $H(q)$ $10 \mu\text{m}$ from the coverslip. Our measured $S(q)$ is excellent; the PY prediction again conforms closely to the data, as shown with solid curves and symbols in Fig. 3(c). By contrast, particles deep in the sample cannot be resolved above the noise; therefore, $S(q)$ from 3D particle positions fails completely, as shown with the dashed curve in Fig. 3(c).

Probing deeply within multiply scattering, dense samples could allow ConDDM to characterize systems that change too rapidly for traditional microscopy-based object tracking [6] and are too dense for DLS and DDM. We explore this capability in swimming bacteria, which have been characterized on the microscopic level with many techniques [11,12] including DDM [6] but only in

2D or in dilute concentrations. To our knowledge, no study has investigated rapid dynamics of bacteria at higher density [12–14] free to swim in 3D, with sufficiently high resolution to resolve individual organisms. To investigate such behavior, we image dense, macroscopically opaque suspensions of *Bacillus subtilis*, a flagellated bacterium, collecting images of 256×128 pixels at 100.0 fps with the point-scanning confocal at various depths from the coverslip; we maintain the sample at 37°C . Near the coverslip, we observe that bacteria move in a 2D plane, their long axes aligned parallel to the coverslip, shown in the inset in Fig. 4(a). Here, each calculated $g(q, \delta t)$ is not exponential, as for diffusing particles, but has a different functional form for each value of q , as shown in Fig. 4(a); there is no universal scaling, and $\tau(q)$ does not follow a simple power law but is instead a sigmoidal curve, shown with open circles in Fig. 2.

By contrast, deeper within the bulk of the sample, the bacteria do not swim within a single plane, and their axes appear to be distributed randomly, shown in the inset in Fig. 4(b). We again find that $g(q, \delta t)$ is not simply exponential. However, unlike the surface-constrained bacteria, those swimming in the bulk have dynamics that, surprisingly, can be scaled onto a single master curve, shown with the solid curve in Fig. 4(b): These $g(q, \delta t)$ follow a compressed-exponential form, $g(q, \delta t) = \exp[-(qv_0\delta t)^\gamma]$, where $\gamma = 1.35$ for all depths greater than $4 \mu\text{m}$ from the coverslip; intriguingly, a similar exponent is observed in

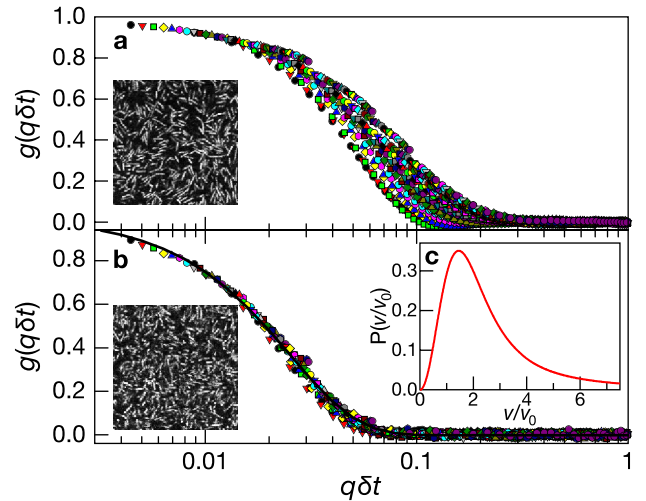


FIG. 4 (color online). (a) $g(q\delta t)$ and \hat{x} - \hat{y} image (inset) for bacteria swimming at the coverslip, for 43 values of q in the range $0.2 < q < 4 \mu\text{m}^{-1}$, each plotted with different symbols, as a function of rescaled time delay $q\delta t$. (b) $g(q\delta t)$ for bacteria swimming deep in the bulk, $16 \mu\text{m}$ from the coverslip, in the same q range as in (a); here, data from all 43 values of q (symbols) scale onto a single master (solid black) curve of the form $\exp[-(qv_0\delta t)^{1.35}]$, with $v_0 = 39.6 \pm 0.3 \mu\text{m/s}$. (Inset) \hat{x} - \hat{y} image of bacteria deep in the bulk, $8 \mu\text{m}$ from the coverslip. (c) Population velocity distribution $P(v/v_0)$ for the bacteria in (b).

aging gels and glasses [15]. Moreover, the resulting $\tau_b(q)$ conform closely to a power law with slope -1 , shown with the open quadrilaterals and dotted line in Fig. 2; this linearity demonstrates that bacteria in the bulk move ballistically over the distances we measure and defines their characteristic speed $\tau_b(q) \sim (v_0 q)^{-1}$; our measured $v_0 = 39.6 \pm 0.3 \mu\text{m/s}$ is consistent with previous measurements in dilute bacterial suspensions [16]. Moreover, we can extract the population's swimming-speed distribution $P(v)$ by inverting $g(q, \delta t) = \langle \exp[i\vec{q} \cdot \vec{v} \delta t] \rangle = \int_0^\infty v P(v) J_0(qv \delta t) dv$, where J_0 is the zeroth-order Bessel function, as shown in Fig. 4(c). By contrast, because $\tau(q)$ does not follow a linear power law for the bacteria swimming near the coverslip, they cannot have a well-defined velocity distribution, contrasting measurements in different bacteria [6]. While the particular numerical values depend on environmental conditions (temperature and nutrients), qualitative differences in scaling demonstrate a fundamentally new measurement using ConDDM and its unique contribution to the study of microorganism motion.

We gratefully acknowledge R. Guerra, T.F. Kosar, D. Luebke, R. Prescott, P. Sims, V. Trappe, B. Calloway, and funding from NASA (NNX08AE09G), the NSF (DMR-1006546), the Harvard MRSEC (DMR-0820484), and NVIDIA.

-
- [1] P.J. Lu, P.A. Sims, H. Oki, J.B. Macarthur, and D.A. Weitz, *Opt. Express* **15**, 8702 (2007).
 [2] P.J. Lu, E. Zaccarelli, F. Ciulla, A.B. Schofield, F. Sciortino, and D.A. Weitz, *Nature (London)* **453**, 499 (2008).

- [3] R. Borsali and R. Pecora, *Soft Matter: Scattering, Imaging and Manipulation* (Springer, Berlin, 2008).
 [4] R. Cerbino and V. Trappe, *Phys. Rev. Lett.* **100**, 188102 (2008).
 [5] F. Giavazzi, D. Brogioli, V. Trappe, T. Bellini, and R. Cerbino, *Phys. Rev. E* **80**, 031403 (2009).
 [6] L.G. Wilson, V.A. Martinez, J. Schwarz-Linek, J. Tailleur, G. Bryant, P.N. Pusey, and W.C.K. Poon, *Phys. Rev. Lett.* **106**, 018101 (2011).
 [7] P.N. Segre, O.P. Behrend, and P.N. Pusey, *Phys. Rev. E* **52**, 5070 (1995).
 [8] A. Robert, J. Wagner, W. Härtl, T. Autenrieth, and G. Grübel, *Eur. Phys. J. E* **25**, 77 (2008).
 [9] C.W.J. Beenaker and P. Mazur, *Physica (Amsterdam)* **126A**, 349 (1984).
 [10] See Supplemental Material at <http://link.aps.org/supplemental/10.1103/PhysRevLett.108.218103> for a simple optical model and numerical calculations demonstrating the accuracy of ConDDM throughout the stated range in q .
 [11] H.P. Zhang, A. Be'er, R.S. Smith, E.L. Florin, and H.L. Swinney, *Europhys. Lett.* **87**, 48 011 (2009)
 [12] A. Sokolov, I.S. Aranson, J.O. Kessler, and R.E. Goldstein, *Phys. Rev. Lett.* **98**, 158102 (2007).
 [13] I. Tuval, L. Cisneros, C. Dombrowski, C.W. Wolgemuth, J.O. Kessler, and R.E. Goldstein, *Proc. Natl. Acad. Sci. U.S.A.* **102**, 2277 (2005).
 [14] A. Sokolov, R.E. Goldstein, F.I. Feldchtein, and I.S. Aranson, *Phys. Rev. E* **80**, 031903 (2009).
 [15] L. Cipelletti, L. Ramos, S. Manley, E. Pitard, D.A. Weitz, E.E. Pashkovski, and M. Johansson, *Faraday Discuss.* **123**, 237 (2003).
 [16] A. Zaritsky and R.M. Macnab, *J. Bacteriol.* **147**, 1054 (1981).